Pure & Appl. Chem., Vol. 59, No. 10, pp. 1285–1294, 1987.
Printed in Great Britain.

Resonance Raman study on the role of the iron-ligand bond for functional activity of heme proteins

Teizo Kitagawa

Institute for Molecular Science, Okazaki National Research Institutes, Myodaiji, Okazaki, 444 Japan

Abstract - A brief description of the resonance Raman study on the role of the iron-ligand bond for the functional activity of heme proteins is presented.

INTRODUCTION

Iron porphyrins in heme proteins are endowed with a specific reactivity toward oxygen in contrast with those in solutions. The reactivity of the heme iron and thus the function of a given heme protein depends on the iron-coordination environments. An essential factor for determining them is the fifth ligand of the heme iron. For instance, cytochrome P-450s with a wide variety of sources and primary structures have in common a cysteinate as the fifth ligand and the identity of the fifth ligand is a distinctive feature of this particular group of proteins. Therefore, elucidation of nature of the ligand is essential for understanding functions of heme proteins.

Oxygen carriers such as hemoglobin (Hb) and myoglobin (Mb) and peroxidases such as horseradish peroxidase (HRP) and cytochrome c peroxidase (CcP) have quite different functions. Nevertheless, both groups of proteins have a histidine residue (His) as the fifth ligand. There must be some features characteristic of each group of proteins with regard to the iron coordination environments. The iron-ligand stretching Raman line, if identified, is expected to serve as the most sensitive probe of the iron coordination environments. In this laboratory we have made efforts to assign the iron-ligand stretching Raman line of various heme proteins and to understand structural implications of the observed frequencies. These results are summarized here and discussion will be focused on the following points; a role of the Fe-His bond in the cooperative oxygen binding of Hb, a distinctive property of the proximal histidine of peroxidases, and a character of the Fe^{IV}=O bond of HRP Compound II. Comprehensive reviews on these subjects are published elsewhere (ref. 1 and 2).

HEMOGLOBIN

Cooperativity and Fe–His stretching vibration

The oxygen binding curve of a single Hb preparation in a given solution can usually be simulated satisfactorily by the two state model (ref. 3). This theory postulates the transition between two alternative quaternary structures having different oxygen affinities. As illustrated in Fig. 1, weak inter-subunit bonding leads to a relaxed tertiary structure of protein, giving rise to the high affinity state, and conversely, strong inter-subunit bonding induces the formation of intra-subunit hydrogen bonds and brings about a tensed tertiary structure, lowering the oxygen affinity (ref. 4). It has long been a matter of debate how a change in the inter-subunit bonding is communicated to the oxygen binding site to lower or raise the oxygen affinity. Perutz (ref. 5) proposed that the tensed structure of the protein might pull the proximal histidine away from the porphyrin plane and accordingly stretch the Fe-His bond.

The presence of the strain in the Fe-His bond of the low affinity deoxyHb has been demonstrated first by Nagai et al. (ref. 6) from the observation of the resonance Raman (RR) line due to the Fe-His stretching vibration, ν(Fe-His); the low- and high-affinity deoxyHbs give the ν(Fe-His) RR line around 216-218 and 221-223 cm^{-1}, respectively. This was later confirmed by other groups (ref. 7 and 8). The next problem to be solved is whether the magnitude of the strain imposed on the Fe-His bond is a continuous variable and is correlated with the oxygen affinity or not. To answer this, Matsukawa et al. (ref. 9) investigated various mutants of human Hbs. Figure 2 shows resonance Raman spectra of a few mutant deoxyHbs with different levels of oxygen affinity. The ν(Fe-His) line is observed at 215, 214, 220 and 222 cm^{-1} for HbA, Hb Kansas, Hb J Capetown, and Hb Chesapeake, respectively. It became evident that only the ν(Fe-His) frequency was altered with different mutant Hbs while all other Raman lines remained unshifted. The observed ν(Fe-His) frequencies and the equilibrium constant for oxygen binding, K_1 (defined as the dissociation constant for the first oxygen molecule to bind to deoxyHb) of various Hbs are

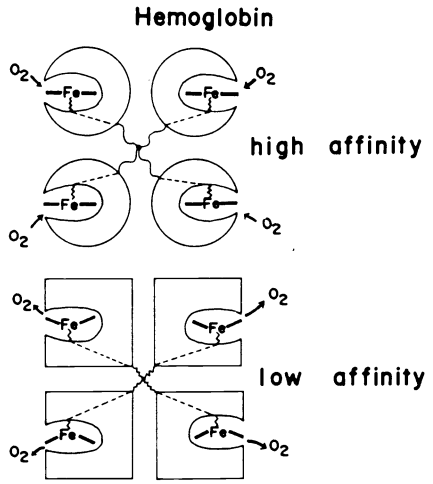

Fig. 1. Two quaternary structures of Hb. The relaxed (R, upper) and tensed (T, lower) structures have the high and low affinity for oxygen, respectively (ref. 4).

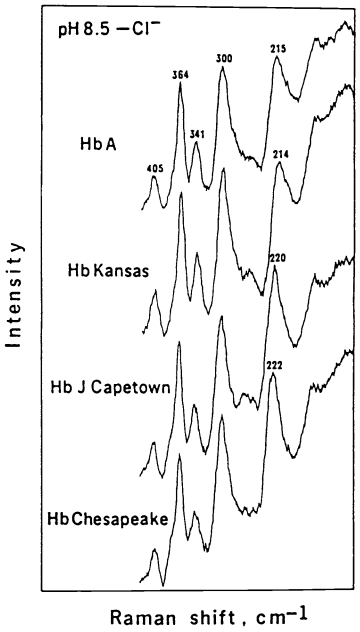

Fig. 2. Resonance Raman spectra of some mutant deoxy Hbs at pH 8.5 in the absence of Cl^-. excitation, 441.6 nm (from ref. 9).

TABLE 1. Observed values of ν(Fe-His) and of K_1 for several hemoglobins

No.[a]	Hemoglobin (Name/Conditions)	ν(Fe-His)[b]	K_1[c]	L[d]	c[e]	K_T	K_R
1.	Hb A/pH 7.0, +IHP[f]	214.5	138	4.5xE8[g]	0.0029	138	0.40
2.	Hb A/pH 7.0, +Cl[h]	215	70	4.35xE7	0.002	70	0.14
3.	Hb A/pH 8.5, +Cl	216	12.5	5.0xE3	0.008	12.5	0.10
4.	Hb A/pH 7.0, -Cl[i]	216	6.06	9.0xE3	0.033	6.06	0.20
5.	Hb A/pH 8.5, -Cl	218	4.9	9.5xE2	0.050	5.0	0.25
6.	Hb J Capetown/pH 7.0, +IHP	214.5	58	9.5xE6	0.0096	58	0.40
7.	Hb J Capetown/pH 7.0, +Cl	215	16.7	2.0xE5	0.012	16.7	0.20
8.	Hb J Capetown/pH 8.5, +Cl	217.5	5.0	5.5xE3	0.04	5.0	0.20
9.	Hb J Capetown/pH 8.5, -Cl	220	1.0		n.d.		
10.	Hb Chesapeake/pH 7.0, +IHP	215	37.1	2.5xE5	0.0166	37.1	0.60
11.	Hb Chesapeake/pH 7.0, +Cl	216	3.52	2.5xE2	0.11	3.64	0.40
12.	Hb Chesapeake/pH 8.5, +Cl	220	1.05	1.2xE1	0.33	1.21	0.40
13.	Hb Chesapeake/pH 8.5, -Cl	222.5	0.60		n.d.		
14.	Hb Kansas/pH 7.0, +Cl	214	50		n.d.		
15.	Hb Kansas/pH 8.5, -Cl	214	19		n.d.		
16.	Hb Yakima/pH 7.0, +IHP	216.5	26.9	5.0xE3	0.026	26.9	0.70
17.	Hb Yakima/pH 7.0, +Cl	220	1.02	2.0xE1	0.36	1.11	0.40
18.	Hb Kempsey/pH 7.0, +IHP	217.5	14.65	9.0xE1	0.070	17.1	1.20
19.	Hb Kempsey/pH 7.0, +Cl	220	1.06	2.0xE1	0.30	1.33	0.40
20.	Hb Hirose/pH 7.0, +IHP	218	11.5		n.d.		
21.	Hb Hirose/pH 7.0, +Cl	219	2.0		n.d.		
22.	Hb Hirose/pH 8.5, +Cl	219	1.3		n.d.		
23.	α chain	223	0.6				
24.	β chain	224	0.34				

[a]Sample Number (ref. 9,10); [b][cm^{-1}]; [c][mmHg]; [d]L=[T]/[R]; [e]$c=K_R/K_T$; [f]in the presence of 1 mM IHP; [g]En means 10^n; [h]in the presence of 0.1 M NaCl; [i]in the absence of chloride ion.

summarized in Table 1, which also includes the MWC parameters determined for the same preparations of Hb as used for the Raman measurements (ref. 10). The ν(Fe-His) frequencies become higher as the oxygen affinity ($1/K_1$) becomes higher.

It is stressed that the Fe-O_2 stretching frequency of oxyHb (ref. 6) and the Fe-CO and C-O stretching frequencies of carbonmonoxyHb (ref. 11) have no correlation with the oxygen affinity, and also that the oxygen binding curves of Hb in various solvent conditions are well simulated by manipulating only one parameter, namely K_T (ref. 12), which is practically the same as K_1. These facts suggest that the key information for cooperativity is contained in deoxyHb, and is therefore consistent with our proposal that the cooperativity is primarily determined by the strain of the Fe-His bond present in the deoxy state. To treat it quantitatively, the following model was proposed.

Continuous strain model for oxygen affinity

Suppose that there are strained and unstrained states regarding the Fe-His bond, and that the low- and high-affinity structures correspond to the strained and unstrained states, respectively. Under the unstrained condition, the Fe-His bond has its intrinsic potential denoted by V_u in Fig. 3. We assume that the potential of the strained Fe-His bond, V_s, is represented by the sum of V_u and W, a contribution from the globin moiety. W is a consequence of the tensed structure of the protein and is therefore considered to produce repulsion for the Fe-His bond. In this treatment V_u and W are approximated by Morse- and de Boer-potentials, respectively.

$$V_u = D_e \{1 - \exp[-\underline{a}(r-r_0)]\}^2 - D_e \quad (1)$$

$$W = \underline{b}\cdot\exp(-\underline{c}r) \quad (2)$$

The stretching force constant (k_u) for the unstrained condition is derived from Eq. 1 as $k_u = 2D_e\underline{a}^2$. The potential minimum of the Fe-His bond under the presence of the strain is shifted to $r_0+\Delta r$ so as to fulfill $d(V_u+W)/dr = 0$. When the strain energy present is defined by $w_0 = \underline{b}\cdot\exp(-\underline{c}r_0)$ (see Fig. 3), then the amount of the stretch of the Fe-His bond is given by

$$\Delta r = w_0\underline{c}/(k_u + w_0\underline{c}^2) \quad (3)$$

and the stretching force constant (k_s) for the strained condition is represented as $k_u(1 - 3\underline{a}\Delta r)$. Therefore, the difference between k_u and k_s is

$$k_u - k_s = 3k_u\underline{a}\Delta r \tilde{=} 3\underline{a}w_0\underline{c} \quad (4)$$

which is related to the frequency shift ($\Delta\nu = \nu_u - \nu_s$) by

$$k_u - k_s = 4\pi^2 c_0^2\mu(\nu_u^2 - \nu_s^2) = 2k_u\Delta\nu/\nu_u \quad (5)$$

where c_0 and μ is the light velocity and the reduced mass, respectively. The bond-energy reduction, ΔQ, of the Fe-His bond upon the stretch by Δr is equal to $w_0(1-\underline{c}\Delta r)$, and when this is combined with Eqs. 4 and 5, the resultant equation is represented as,

$$\Delta Q = p_1\Delta\nu + p_2\Delta\nu^2 \quad (6)$$

where $p_1 = (2k_u)/(3\underline{a}\underline{c}\nu_u)$ and $p_2 = -(4k_u)/(9\underline{a}^2\nu_u^2)$.

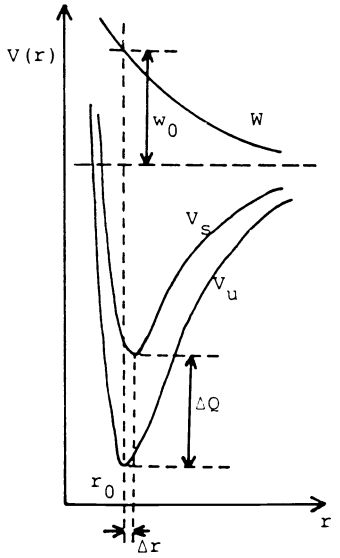

Fig. 3. Schematic diagram for the potential functions of the unstrained (V_u) and strained (V_s) Fe-His bonds. W stands for the repulsive potential caused by strain of globin. Δr denotes the difference in the potential minima of V_s and V_u.

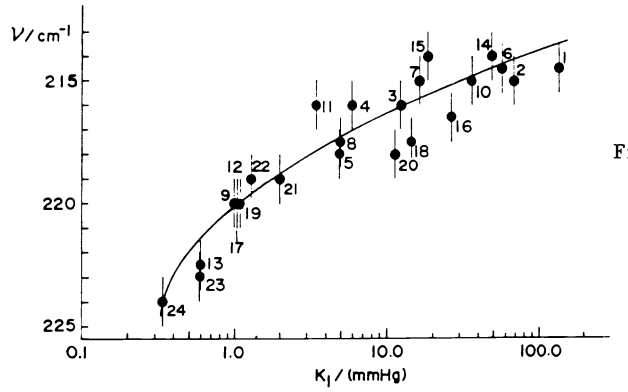

Fig. 4.
The ν(Fe-His) vs K_1 plots for various human mutant deoxy Hbs. The solid line denotes the curve of $\nu = 225.2 - 7.10(\log_{10}K_1 - 0.488)^{\frac{1}{2}}$ (see Eq. 9). The numbers stand for the samples specified in Table 1 (from ref. 9).

On the other hand, the oxygen affinity is determined by a change of free energy upon binding of oxygen. The difference between the oxygen affinities of the unstrained and strained structures were previously related to ΔQ through Eq. 7 (ref. 9),

$$RT\cdot\ln(K_1^{S}) - RT\cdot\ln(K_1^{U}) = \kappa\Delta Q \tag{7}$$

where κ is a proportionality constant and K_1^{U} and K_1^{S} are K_1 of the unstrained and strained conditions, respectively. Since K_1^{U} should be a constant, we put $RT\cdot\ln(K_1^{U}) = \gamma$. Combining Eq. 6 with Eq. 7 results in Eq. 8,

$$\Delta\nu = -(p_1/2p_2) + \{(p_1^2/4p_2^2) + [RT\cdot\ln(K_1^{S}) - \gamma]/(\kappa p_2)\}^{\frac{1}{2}} \tag{8}$$

and thus Δν can be correlated with K_1^{S}. In accord with it, the observed ν_s were fitted with Eq. 9,

$$\nu_s = q_1 + q_2[\log(K_1^{S}) + q_3]^{\frac{1}{2}} \tag{9}$$

where q_1, q_2 and q_3 are adjustable parameters. The ν(Fe-His) frequencies of various human deoxyHbs are plotted against K_1 in Fig. 4, where the solid line represents the theoretical curve calculated from Eq. 9.

Despite the crude approximation, the calculated curve well reproduces the observed results. This might imply the validity of the present strain model. In this treatment, the frequency difference between the α and β subunits was neglected. However, the Raman data suggest that the magnitude of the strain imposed to the Fe-His bond is three times larger in the α than the β subunit (ref. 13,14). Since the RR intensity of the ν(Fe-His) line of the α subunit becomes weaker as its frequency becomes lower, while that of the β subunit remains almost unaltered, it is fairly difficult to infer an average of the α and β subunits from the RR spectra shown in Fig. 2. Anyhow, the difference between the α and β subunits should be incorporated in a refined treatment of the strain model.

PEROXIDASE

Heme-linked ionization and the Fe–His stretching mode

Peroxidase is an enzyme that catalyzes the oxidation of various organic molecules by H_2O_2 as their specific oxidant (see ref. 15 for a review). Although both HRP and Mb have a histidine-coordinated iron-protoporphyrin, an oxygen molecule bound to ferroHRP is quickly reduced to water, but that bound to deoxyMb is quite stable. The resonance Raman spectra of the two proteins in the reduced state are compared in Fig. 5(A). The two spectra in the 1200-1700 cm^{-1} region are alike and of typical five-coordinate high-spin type. However, they are different in the lower frequency region.

Teraoka and Kitagawa (ref. 16) assigned the Raman line of ferroHRP at 244 cm^{-1} to the ν(Fe-His) mode from the experiment on ^{54}Fe isotope substitution. The frequency of the ν(Fe-His) line of ferroHRP exhibited appreciable pH dependence while all other lines showed no pH dependence. This is illustrated in Fig. 5(B), where data of two isozymes (HRP-A and HRP-C) are included. The midpoint pH for the frequency shift is in close agreement with the pK_a values of the heme-linked ionization determined with other techniques (ref. 15). Accordingly, the ν(Fe-His) frequency can be used as a probe of the heme-linked ionization for peroxidases. Teraoka et al. (ref. 17) measured the ν(Fe-His) modes of other plant peroxidases including several isozymes of turnip and Japanese-radish peroxidases and found that all the ν(Fe-His) modes exhibit the pH-dependent frequency shift around neutral pH. However, the ν(Fe-His) mode of deoxyMb showed no pH-dependent frequency shift between pH 4.7 and 11.8. Therefore, the pH dependence of the ν(Fe-His) frequency was concluded to be a characteristic property of peroxidases.

Iron-coordination environments

In Fig. 5(A), the ν(Fe-His) frequency of ferroHRP (244 cm^{-1}) is higher than that of deoxyMb (220 cm^{-1}). The higher ν(Fe-His) frequency seems to be a general trend of all peroxidases so far examined. To understand its implications, 2-methylimidazole (2-MeIm) complex of iron protoporphyrin [Fe^{2+}(PP)(2-MeIm)] was examined. The assignment of the Fe-(2-MeIm) stretching mode [ν(Fe-(2-MeIm))] of the model complexes has been established from the isotope substitution experiment (ref. 18). The solvent effect of the ν(Fe-(2-MeIm)) mode of Fe^{2+}(PP)(2-MeIm) is illustrated in the left panel of Fig. 6. The ν(Fe-(2-MeIm)) line is observed at 219 cm^{-1} for Fe^{2+}(PP)(2-MeIm) in a simple aqueous solution, but is shifted to 209 cm^{-1} in the presence of detergent and further to a lower frequency in an organic solvent as shown at the bottom. This suggests that destruction of hydrogen bond between the N_1-hydrogen of bound 2-MeIm and solvent H_2O or excess 2-MeIm molecules upon micelle formation by detergent lowers the basicity of the N_3 atom of 2-MeIm and thus weakens the Fe-(2-MeIm) bond.

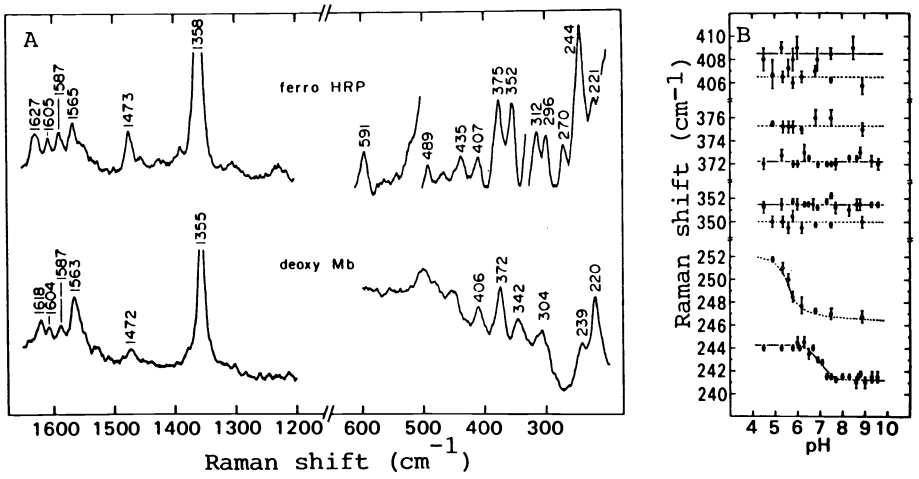

Fig. 5. A) Resonance Raman spectra of ferro HRP (upper) and deoxy Mb (lower) excited at 457.9 nm. B) pH dependence of frequencies of a few selected Raman lines of ferro HPR; solid lines, isozyme C; broken lines, isozymes A (from ref. 16).

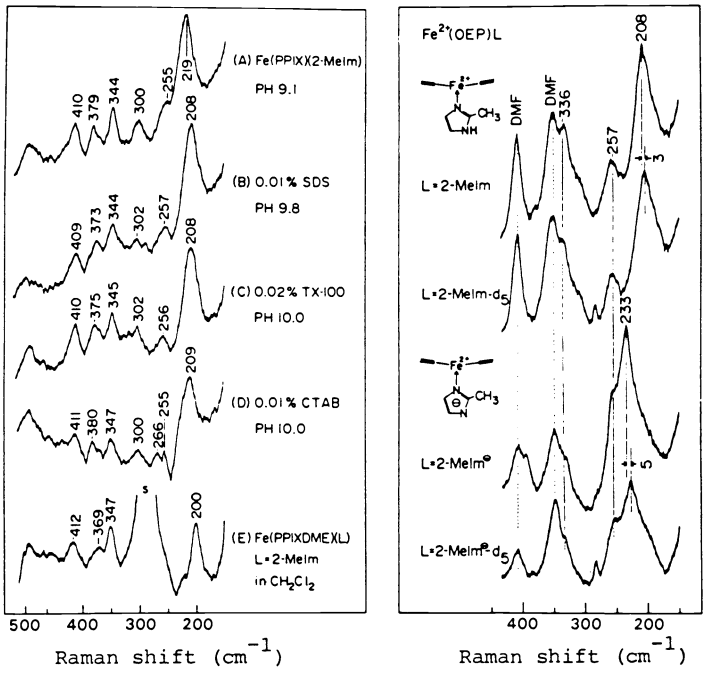

Fig. 6. (Left) Resonance Raman spectra of five-coordinate high-spin Fe^{II}(PP) with 2-MeIm as an axial ligand in pure- (A) 0.01% SDS- (B), 0.02% Triton X 100- (C), and 0.01% CTAB-aqueous solutions and in CH_2Cl_2 (E). Protoporphyrin IX dimethylester is used for (E). (Right) Resonance Raman spectra of five-coordinate high-spin Fe^{II} (OEP) with 2-MeIm (upper) or 2-MeIm$^-$ (lower) as the axial ligand. The spectra from complexes with perdeuterated 2-MeIm or 2-MeIm$^-$ are also shown below each spectrum (from ref. 16).

TABLE 2. Fe(II)-histidine stretching frequencies of various hemoproteins [cm^{-1}]

	Acidic		Alkaline	Mid pH	Ref.
peroxidases					
CcP	247		234	7.3	a
HRP-A_2	252		246	5.5	b
HRP-C	244		241	7.0	b
TP-1	252		248	6.3	c
TP-3	251		246	5.9	c
TP-7	248		244	6.1	c
JRP-2	247		243	6.3	c
JRP-3	252		248	6.5	c
JRP-9	245		241	7.1	c
JRP-15	246		242	6.7	c
JRP-16	250		246	6.8	c
LP		258			d
IP		254			e
oxygen carriers					
deoxy Mb		220			f
deoxy Hb A		216			g
NES des-Arg Hb		220			g
giant Hb		221			h
cytochrome c oxidases					
bacterium HB 8		210			i
bacterium PS 3		213			j
bovine heart		214			i
yeast		220			i

[a]this work; [b]Teraoka and Kitagawa (1981); [c]Teraoka et al. (1983); [d]Hashimoto (1984); [e]Kimura et al. (1981); [f]Kitagawa et al. (1979); [g]Nagai and Kitagawa (1980); [h]Kitagawa et al. (1984); [i]Ogura et al. (1983); [j]Ogura et al. (1984).

If this idea is valid, the ν(Fe-(2-MeIm)) frequency is expected to shift to a higher frequency upon deprotonation of 2-MeIm, because the deprotonated 2-MeIm can be regarded as the extreme of 2-MeIm with the strongest hydrogen bond. The results of the experiments for examining the validity of that idea are shown in the right panel of Fig. 6 (ref. 16). The 208 cm^{-1} line of Fe^{2+}(OEP)(2-MeIm)(OEP: octaethyl porphyrin) and the 233-cm^{-1} line of Fe^{2+}(OEP)(2-MeIm^-) exhibit the isotope frequency shift upon perdeuteration of 2-MeIm (2-MeIm-d_5), and are therefore assigned to the Fe^{2+}-(2-MeIm) and Fe^{2+}-(2-MeIm^-) stretching modes, respectively. This means that the Fe^{2+}-(2-MeIm) stretching mode is shifted to a higher frequency by 25 cm^{-1} upon deprotonation of 2-MeIm. This trend had previously been recognized by Stein et al. (ref. 19) who tried to interpret the quaternary structure-dependent change of the ν(Fe-His) frequency in terms of the hydrogen bonding of the proximal histidine.

The size of the frequency shift observed for deprotonation of 2-MeIm is remarkably close to the difference between the ν(Fe-His) frequencies of deoxyMb and ferroHRP (24 cm^{-1}, see Fig. 5), suggesting that the imidazole proton of the proximal histidine of HRP is very strongly hydrogen-bonded to neighboring amino acids (ref. 16). This is consistent with the NMR study that identified the paramagnetically shifted N_δ-proton of proximal histidine (ref. 20). Unfortunately, however, there has been no x-ray data for HRP. Among peroxidases, the x-ray crystallographic data is available only for yeast CcP (ref. 21). Therefore, Hashimoto et al. (ref. 22) extended similar measurements to CcP and assigned the Raman line of ferroCcP at 247 cm^{-1} to the ν(Fe-His) mode on the basis of the ^{54}Fe isotopic shift. This frequency is similar to the ν(Fe-His) frequencies of other peroxidases but is distinctly higher than those of oxygen carriers. On the other hand, the presence of the strong hydrogen bond for the proximal histidine has been established with CcP (ref. 21). Consequently, the coordination of negatively charged imidazole to the heme iron at the fifth coordination site is considered to be a feature characteristic of all peroxidases but is distinct from oxygen carriers. The ν(Fe-His) frequencies of all heme proteins so far clarified are listed in Table 2.

Fe^{IV}=O stretching mode of compound II

The characteristic property of a peroxidase is seen in its catalytic mechanism (ref. 15). The native ferric enzyme is oxidized by H_2O_2 into Compound I, which is then reduced twice by substrates to the native enzyme through Compound II as an intermediate. Accordingly, Compound II is higher by one oxidative equivalent than native enzyme. Identification of the sixth ligand of Compound II has been a matter of spectroscopic concern; a hydroxy ligand was favored from the biochemical side (ref. 15) but the oxo-ferryl structure was proposed by NMR (ref. 23) and ENDOR (ref. 24) studies.

Recently, Hashimoto et al. (ref. 25) and Terner et al (ref. 26) independently succeeded in observing the Fe^{IV}=O stretching Raman line [ν(Fe=O)] of HRP Compound II. The results of Hashimoto et al (ref. 25) are shown in Fig. 7, where the resonance Raman spectra of HRP Compound II derived from ^{54}Fe-HRP/$H_2{}^{16}O_2$ (B), ^{56}Fe-HRP/$H_2{}^{16}O_2$ (C), and ^{56}Fe-HRP/$H_2{}^{18}O_2$ (D) are displayed. The spectrum at the top (A) is of native enzyme. In comparison with this, the ordinary Compound II (^{56}Fe-HRP/$H_2{}^{16}O_2$) (spectrum C) gives rise to a new Raman line at 787 cm^{-1}, which is shifted to a higher frequency by 3 cm^{-1} upon ^{54}Fe substitution (spectrum B), and to a lower frequency by 34 cm^{-1} upon ^{18}O substitution (spectrum D). These isotopic frequency shifts closely agree with those expected for the Fe=O two-body harmonic vibration (+3.3 and -35 cm^{-1} for the ^{54}Fe and ^{18}O substitutions, respectively). This line exhibits no frequency shift upon deuterium substitution as shown by spectrum E, indicating the absence of an exchangeable proton attached to the sixth ligand. Terner et al. (ref. 26) reached the same conclusion as described here, although they did not carry out the ^{54}Fe isotope substitution experiment. Consequently, the Raman studies rule out the Fe^{IV}-OH structure. The ν(Fe=O) frequency of Compound II is significantly lower than that of the five-coordinate Fe^{IV}=O porphyrin complex (852 cm^{-1}) (ref. 27), presumably due to the trans effect of the negatively charged imidazole ligand. It is worth noting that the ν(Fe=O) Raman line is detectable only in the initial few minutes of observation even with a spinning cell and a very low laser power (10 mW at 406.7 nm) (ref. 25). Therefore, in spite of considerable efforts, its observation has not been possible until OMA was available to Raman experiments.

Oxygen exchange of Fe^{IV}=O heme

The pK_a of the heme-linked ionization of Compound II is shifted to 8.6. To see the effect of its protonation, Hashimoto et al (ref. 28) examined the resonance Raman spectra of Compound II at neutral pH. The spectra of Compound II at pH 7.0 derived from four combinations of $H_2{}^{18}O_2$ or $H_2{}^{16}O_2$ and $H_2{}^{18}O$ or $H_2{}^{16}O$ are displayed in Fig. 8. When Compound II is formed with $H_2{}^{16}O_2$ in ordinary water ($H_2{}^{16}O$), a new line appears at 774 cm^{-1} (b). Contrary to the results shown in Fig. 7, the 774 cm^{-1} line exhibits no frequency shift upon replacement of $H_2{}^{16}O_2$ with $H_2{}^{18}O_2$ (c). However, when water is replaced with $H_2{}^{18}O$ without changing H_2O_2 with the isotope, intensity of the 774 cm^{-1} line reduces significantly and a new line appears at 740 cm^{-1} (d). When the ^{18}O isotope is used for both water and hydrogen peroxide, the 774-cm^{-1} line disappears completely (e), while the 740 cm^{-1} line remains.

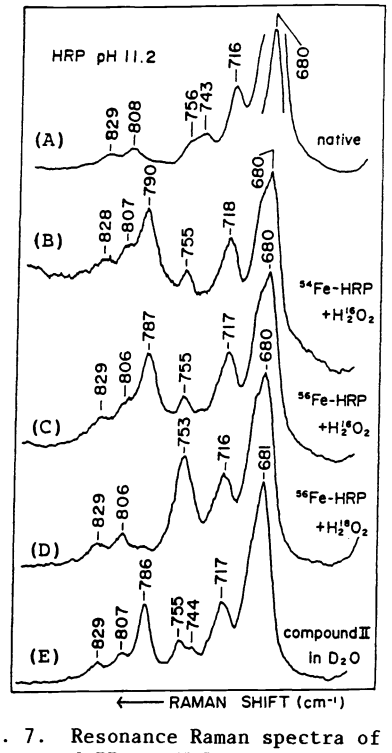

Fig. 7. Resonance Raman spectra of HRP Compound II at pH 11.2. Top is for the native enzyme and others are for Compound II with isotope substitutions specified at right side of each spectrum; excitation, 406.7 nm, 10 mW, accumulation, 3 min (ref. 25).

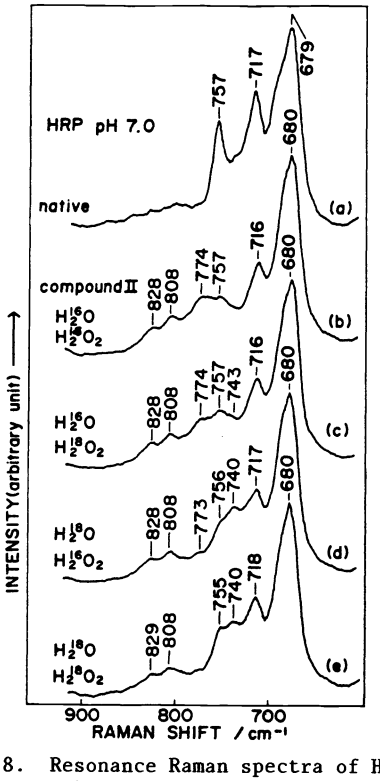

Fig. 8. Resonance Raman spectra of HRP Compound II at pH 7.0. Top is for the native enzyme and other are for Compound II derived from $H_2{}^{16}O_2$ or $H_2{}^{18}O_2$ in $H_2{}^{16}O$ or $H_2{}^{18}O$; excitation 406.7 nm, 10 mW, accumulation, 3 min (ref. 28).

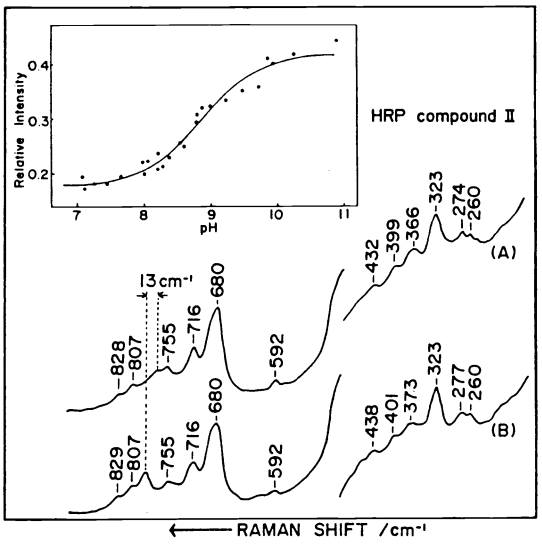

Fig. 9. Resonance Raman spectra in the 200- to 900-cm^{-1} region of Compound II in H_2O. The upper and lower frequency regions were obtained in an identical exposure but are represented separately to adjust background levels. Spectrum A, pH 7.0; spectrum B, pH 11.2; excitation, 406.7 nm, 10 mW; accumulation, 2 min. Inset; pH dependent intensity change of the Fe^{IV}=O stretching Raman line of Compound II in H_2O. The maximum intensities at 787 cm^{-1} relative to those at 680 cm^{-1} are plotted against pH. The solid line is a theoretical curve expected for dissociation of one proton with pK_a = 8.8.

On the analogy of the results at alkaline pH, the new line of Compound II at 774 cm^{-1} is considered to arise from the ν(Fe=O) mode. The fact that this line exhibits the isotopic frequency shift for $H_2{}^{18}O$ strongly suggests that the heme bound oxygen is unexpectedly exchanged with an oxygen atom of bulk water. This kind of exchange reaction no longer takes place at pH 11.2, where the enzymic activity is lost. Therefore, the oxygen exchange seems to be directly involved in the enzymic catalysis.

Upon protonation of a particular residue involved in the heme-linked ionization, the ν(Fe=O) line shifts to a lower frequency from 787 to 774 cm^{-1}. This feature is demonstrated in Fig. 9, where RR spectra of Compound II in H_2O at pH 7 (A) and at pH 11.2 (B) are shown. Since the intensity of the Raman line at 680 cm^{-1} is not altered by the pH change, the intensity of the 786 cm^{-1} line relative to that of the 680 cm^{-1} line was plotted against pH in the inset of Fig. 9. This plot can be well fitted by a theoretical curve (solid line) calculated for ionization of a residue with pK_a = 8.8; this value is in close agreement with the reported pK_a value (= 8.6) for the heme-linked ionization of Compound II (ref. 15). On the other hand, the RR spectra in the lower frequency region (350-200 cm^{-1}) in Fig. 9 are nearly identical in the two solutions at pH 7 and 11.2. This would suggest that the protein-heme interactions, including the Fe-His bond, are altered little by a pH change. Therefore, the lower frequency of the ν(Fe=O) mode in neutral solutions compared with alkaline solutions probably suggests the presence of a hydrogen bond between the heme-bound oxygen and the protonated form of the residue involved in the heme-linked ionization, probably distal histidine. This is consistent with the fact that the ν(Fe=O) frequency is slightly higher in D_2O than in H_2O at neutral pH while there is no difference at alkaline pH (ref. 28,29).

A model of the active site of Compound II deduced from this study is schematically illustrated in Fig. 10. The heme-linked ionization ($A \rightleftarrows B$) of the native enzyme occurs with pK_a = 5.5 (ref. 15). The deprotonated native form (Fig. 10, step A) reacts with H_2O, giving rise to protonated Compound II (step D). The strength of the Fe^{IV}=O bond as well as the heme structure are nearly the same for step D at pH 7 and for step E at 11.2 except for the presence of the weak hydrogen bond in neutral solutions. Nevertheless, the heme-bound oxygen atom in D at pH 7 is rapidly exchanged with bulk water but that in E at pH 11 is not exchanged at all. Therefore, it seems that the hydrogen bonded proton in D plays an essential role in the exchange phenomenon. In the absence of this proton at alkaline pH, the enzyme is inactive. Presumably, the heme-bound oxygen and the hydrogen-bonded proton combine and exchange with bulk water through structure C. This exchange reaction continues until an electron is donated by a substrate. Although such an oxygen exchange has never been suggested for HRP, and Terner et al (ref. 29) did not notice this phenomenon in their RR study of Compound II, this was observed for isozyme A of HRP at an acidic side of its

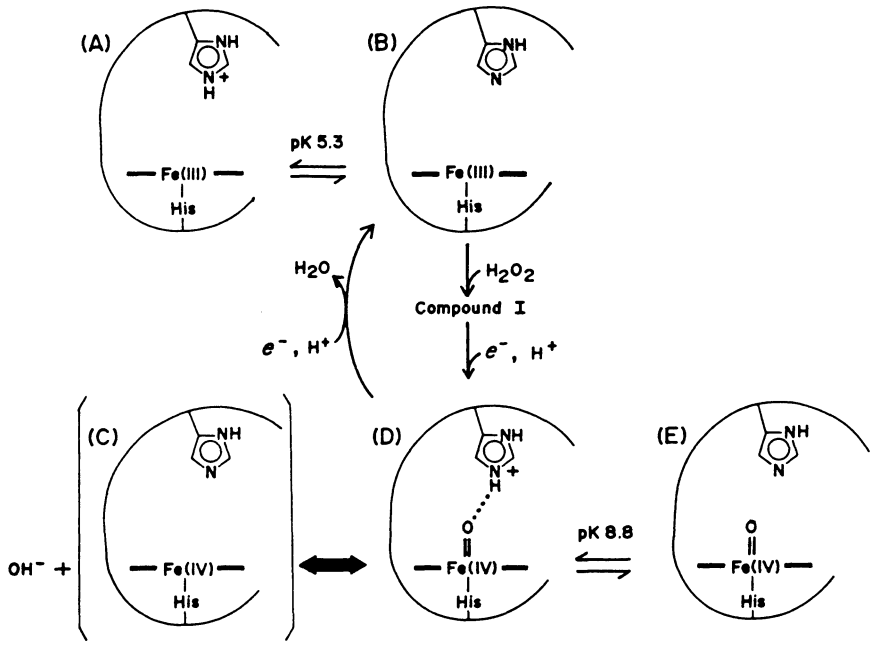

Fig. 10. Schematic diagram for molecular mechanism of HRP catalysis. A↔B represents the equilibrium for the heme-linked ionization in the native ferric form, and D↔E represents that for Compound II. C↔D represents a hypothetical mechanism for the oxygen exchange between the Fe^{IV}=O heme and bulk water. In this figure, distal histidine is considered to be responsible for the heme-linked ionization. In the acidic form of Compound II (D), the proton of distal histidine is hydrogen bonded to the heme-bound oxygen (O^{2-}) and they combine to yield a hydroxy anion upon the oxygen exchange reaction (C).

heme-linked ionization (ref. 30) and for Compound ES of CcP (ref. 22). The rate of the oxygen exchange seemed larger for isozyme A than for isozyme C. This is compatible with the lower pK_a value of isozyme A, when the dissociation of the proton is the rate-limiting step for the oxygen exchange. A similar oxygen exchange is also reported for peroxidase reaction of cytochrome P-450 (ref. 31) and its model compound with the Fe^{IV}=O heme (ref. 32). It is stressed here that the exchange phenomenon is not an intrinsic property of the Fe^{IV}=O heme but is enabled by participation of a hydrogen-bonded proton in the catalysis.

Acknowledgement

The author is grateful to Drs. S. Matsukawa (Kanazawa Univ.), K. Nagai (Medical Research Council, UK), H. Hori (Osaka Univ.), K. Mawatari (Kanazawa Univ.), T. Yonetani (Univ. of Pennsylvania), I. Yamazaki (Hokkaido Univ.), T. Tatsuno (Osaka Univ.), J. Teraoka (Osaka City Univ.), S. Hashimoto (IMS) and T. Ogura (IMS), since the results described here were obtained in collaboration with them.

REFERENCES

1. T. Kitagawa, in "Resonance Raman Investigation of Biomolecules", (T. G. Spiro, ed.), 3, Wiley & Sons, in press.
2. T. Kitagawa, in "Advances in Infrared and Raman Spectroscopy", (R.J.H. Clark and R.E. Hester, eds.), 13, pp. 443-481 (1986).
3. J. Monod, J. Wyman, J.P. Changeux, J. Mol. Biol., 12, 88 (1965).
4. M.F. Perutz, Nature, (London), 228, 726 (1970).
5. M.F. Perutz, Nature, (London), 273, 495 (1972).
6. K. Nagai, T. Kitagawa and H. Morimoto, J. Mol. Biol., 136, 271 (1980).
7. A. Desbois, M. Lutz and R. Banerjee, Biochim. Biophys. Acta, 671, 177 (1981).
8. M.R. Ondrias, D.L. Rousseau, J.A. Shelnutt, and S.R. Simon, Biochemistry, 21, 3428 (1982).
9. S. Matsukawa, K. Mawatari, Y. Yoneyama and T. Kitagawa, J. Am. Chem. Soc., 107, 1108 (1985).

10. S. Matsukawa, K. Mawatari, Y. Shimokawa, and Y. Yoneyama, J. Mol. Biol., 150, 615 (1981).
11. D.L. Rousseau, S.L. Tan, M.R. Ondrias, S. Ogawa, R.W. Noble, Biochemistry, 23, 2857 (1984).
12. K. Imai, J. Mol. Biol., 167, 741 (1983).
13. K. Nagai and T. Kitagawa, Proc. Natl. Acad. Sci. USA, 77, 2033 (1980).
14. M.R. Ondrias, D.L. Rousseau, T. Kitagawa, M. Ikeda-Saito, T. Inubushi and T. Yonetani, J. Biol. Chem., 257, 8766 (1982).
15. I. Yamazaki, M. Tamura and R. Nakajima, Mol. Cell. Biochem., 40, 143 (1981).
16. J. Teraoka and T. Kitagawa, J. Biol. Chem., 256, 3969 (1981).
17. J. Teraoka, D. Job, Y. Morita and T. Kitagawa, Biochim. Biophys. Acta, 747, 10 (1983).
18. H. Hori and T. Kitagawa, J. Am. Chem. Soc., 102, 3608 (1980).
19. P. Stein, M. Mitchell and T.G. Spiro, J. Am. Chem. Soc., 102, 7795 (1980).
20. G.N. LaMar and J.S. deRopp, Biochem. Biophys. Res. Commun., 90, 36 (1979).
21. T.L. Poulos, S.T. Freer, R.A. Alden, S.L. Edwards, U. Skogland, K. Takio, B. Eriksson, N. Xuong, T. Yonetani and J. Kraut, J. Biol. Chem., 255, 575 (1980).
22. S. Hashimoto, J. Teraoka, T. Inubushi, T. Yonetani and T. Kitagawa, J. Biol. Chem., 261, 1110 (1986).
23. G.N. LaMar, J.S. deRopp, L. Latos-Grazynski, A.L. Balch, R.B. Johnson, K.M. Smith, D.W. Parish and R. Cheng, J. Am. Chem. Soc., 105, 782 (1983).
24. J.E. Roberts, B.M. Hoffman, R. Rutter and L.P. Hager, J. Am. Chem. Soc., 103, 7654 (1981).
25. S. Hashimoto, Y. Tatsuno and T. Kitagawa, Proc. Japan Acad., 60, Ser B, 345 (1984).
26. J. Terner, A.J. Sitter and C.M. Reczek, Biochim. Biophys. Acta, 828, 73 (1985).
27. L. Bajor and K. Nakamoto, J. Am. Chem. Soc., 106, 3045 (1984).
28. S. Hashimoto, T. Tatsuno and T. Kitagawa, Proc. Natl. Acad. Sci. USA, 83, 2417 (1986).
29. A.J. Sitter, C.M. Reczek and J. Terner, J. Biol. Chem., 260, 7515 (1985).
30. S. Hashimoto, R. Nakajima, I. Yamazaki, Y. Tatsuno and T. Kitagawa, FEBS Letts., in press.
31. G.D. Nordblom, R.E. White and M.J. Coon, Arch. Biochem. Biophys., 175, 524 (1976).
32. J.T. Groves, R.C. Haushalter, M. Nakamura, T.E. Nemo and B.J. Evance, J. Am. Chem. Soc., 103, 2884 (1981).